Batteries & Supercaps

Research Article
doi.org/10.1002/batt.202400139

Chemistry Europe
European Chemical Societies Publishing

www.batteries-supercaps.org

Triblock Polymer/Acetylene Black Dual-Assisted Preparation of Ge/C Nanocomposites with Superior Lithium Storage Performance

Mingming Zhang,[a, b] Kuan Shen,[b] Mingyue Gao,[b] Xingmei Guo,*[a, b] Junhao Zhang,*[b] Hongxing Gu,*[c] Qinghong Kong,[d] and Zhong Jin*[a]

Anode materials based on IV main group elements like Si, Ge, and Sn show great potential for lithium-ion batteries (LIBs) due to their high specific capacity and low working potential. However, issues such as volume expansion and lattice pulverization hinder their practical usage. To address these issues for Ge, a novel F127 triblock polymer/acetylene black dual-assisted strategy is proposed to achieve uniform dispersion of polycrystalline Ge, enabling the preparation of Ge@C nanocomposites via hydrogen reduction. The introduced F127 triblock polymer and acetylene black serves a dual purpose to enhance electrical conductivity and prevent Ge nanoparticles from agglomeration. When tested as anode material for LIBs, the Ge@C nanocomposites exhibit exceptional electrochemical performances, demonstrating a sustained specific discharge capacity of 780 mA h g^{-1} at 0.2 A g^{-1} after 100 cycles. Moreover, the capacity remains at 767 mA h g^{-1} even after 300 cycles at a higher current density of 0.5 A g^{-1}. These enhanced lithium storage performances are attributed to the combined effects of well-dispersed tiny Ge nanoparticles, uniform carbon coating, and an abundance of defects. These factors effectively mitigate the volume expansion and lattice pulverization of Ge nanoparticles and concurrently enhance their conductivity, leading to improved overall performance in LIBs.

Introduction

Lithium-ion batteries (LIBs) are considered as one of the most promising electrochemical energy storage devices and have been extensively applied in electric vehicles, laptop, energy storage power station, etc.[1] The increasing requirements for the comprehensive properties of power supplies triggers intensive research on high-performance electrode materials for LIBs.[2] Germanium (Ge), an element at the same group with silicon (Si), has a high theoretical capacity of 1623 mA h g^{-1} and is regarded as a promising anode material for LIBs.[3] Compared with Si, Ge has better electrical conductivity, higher Li^+ diffusion coefficient, and smaller volume expansion after lithium alloying.[4] However, the semiconducting behavior of Ge could still not meet the efficient electron conducting requirement of electrodes, and the volume change of pure Ge during charging-discharging could still cause pulverization, which lead to capacity loss and inhibit direct use of Ge as LIB anodes.[5] Besides, the rareness of elemental Ge in the natural state also hinders its widespread application.

To address the above-mentioned problems, researchers have undertaken a series of investigations: (1) Constructing Ge-based anode materials into nanoscale or porous structures to mitigate volume changes during charging-discharging;[6] (2) Applying protective coatings on Ge-based anodes to shield from direct contact with the electrolyte and avoid structural collapse;[7] (3) Introducing carbonaceous components to prepare Ge/carbon composites to improve the conductivity as well as structural stability.[8] Among them, combining with carbon is simple and efficient. The presence of carbon minimizes the mechanical stress caused by volume expansion of Ge in the electrochemical process. However, current methods for obtaining Ge/C composites are usually tedious and could not bypass the intractable problem of scarce Ge resources in elementary state. Although germanium dioxide (GeO_2) is common in nature, the crystalline structure and particle size are relatively large, which makes it difficult to disperse into nanometer size.[9] Exploring a facile approach to obtain tiny Ge nanoparticles from ordinary GeO_2 and coating them with carbon would be an optimum strategy to achieve high lithium storage performance,

[a] M. Zhang, Dr. X. Guo, Prof. Z. Jin
MOE Key Laboratory of Mesoscopic Chemistry, MOE Key Laboratory of High Performance Polymer Materials and Technology, Jiangsu Key Laboratory of Advanced Organic Materials, School of Chemistry and Chemical Engineering
Nanjing University
No. 163 Xianlin Avenue, Nanjing 210023, China
E-mail: guoxm@just.edu.cn
zhongjin@nju.edu.cn

[b] M. Zhang, K. Shen, M. Gao, Dr. X. Guo, Prof. J. Zhang
School of Environmental and Chemical Engineering
Jiangsu University of Science and Technology
No. 2 Mengxi Road, Zhenjiang 212003, China
E-mail: guoxm@just.edu.cn
jhzhang6@just.edu.cn

[c] H. Gu
Jiangsu Hengshen Co., Ltd, Zhenjiang 212314, China
E-mail: guhongxing07@163.com

[d] Dr. Q. Kong
School of the Environment and Safety Engineering
Jiangsu University
No. 301 Xuefu Road, Zhenjiang 212013, China

Supporting information for this article is available on the WWW under https://doi.org/10.1002/batt.202400139

Research Article
doi.org/10.1002/batt.202400139
Chemistry Europe
European Chemical Societies Publishing

which integrates the advantages of nanostructures and carbon coating, while achieving cost reduction.

In this work, triblock copolymer F127 was utilized to disperse commercial GeO_2 polycrystalline microparticles in water to obtain uniform GeO_2/F127 dispersion. This surfactant-assisted dispersion method is economical, efficient and environmentally friendly compared to the conventional approach of dispersing GeO_2 with concentrated ammonia water and strong alkali solution. The results show that the concentration of F127 solution could regulate the dispersion degree of GeO_2. Subsequently, the GeO_2/F127 dispersion was mixed with acetylene black, followed by freeze-drying and high-temperature H_2 reduction to obtain nanosized and carbon-coated Ge (Ge@C) composites. When utilized as anode material for LIBs, the as-synthesized Ge@C composites exhibited excellent cycle stability. This work proposed an innovative method for dispersing commercial GeO_2 polycrystalline particles and realizing facile preparation of Ge@C nanocomposites, which is a successful paradigm with significant demonstrative value for developing advanced LIB anodes.

Results and Discussion

Figures 1(a, b) illustrate that commercial GeO_2 consists of polycrystalline particles with rough surface and micrometer size. Figure1(c) exhibits F127/GeO_2 dispersion with the F127 concentrations of 0 wt%, 1 wt%, 2 wt% and 4 wt%. According to the results, the white precipitate was formed rapidly in the GeO_2 dispersion, indicating the insolubility of GeO_2 in water. Notably, F127 has the ability to disperse GeO_2 microparticles by splitting polycrystallines into tiny crystallites due to their surfactant amphophilic nature. Therefore, the dispersion solution gradually become clear and transparent with the increasing concentration of F127. Only at a concentration of 4 wt% F127, complete dispersion of 0.1 g GeO_2 polycrystalline microparticles in 20 mL water was achieved. As shown in Figure 1(d), the SEM image indicates that GeO_2 polycrystalline microparticles have been dispersed to single crystal nanoparticles in F127 solution. Compared to the previously reported method for dispersing GeO_2 with concentrated ammonia or sodium hydroxide solution, a more economical, effective and environmentally friendly approach was discovered.[10] Figure 1(e) shows the SEM image of Ge@C(H_2/Ar) nanocomposite obtained through high-temperature H_2 reduction in H_2/Ar mixed atmosphere. The results reveal that the surface of Ge@C(H_2/Ar) is rough, primarily due to the more efficient thermal reduction of the precursor in the H_2/Ar mixed atmosphere. This rough surface on Ge@C(H_2/Ar) is conducive to electrolyte wetting and accelerate Li^+ transport, effectively improving the lithium storage performance.[11] The weight ratio of carbon in Ge@C(H_2/Ar) was estimated to be 39.2 wt% accoriding to the thermogravimetric analysis (Figure S1).To further elucidate the internal structure of Ge@C(H_2/Ar), the low-magnification TEM image is presented in Figure 1(f), which reveals that the size of a single Ge@C(H_2/Ar) particle is 2~3 μm, and Ge nanoparticles are uniformly dispersed in carbon matrix. The carbon protection layer serves to prevent the pulverization of Ge nanoparticles caused by Ge volume changes and enhance the conductivity. Figures 1(g, h) display the HRTEM images of Ge@C(H_2/Ar) nanocomposites. The identified lattice spacing of 0.326 nm aligns with the (111) plane of Ge, offering conclusive evidence for the presence of Ge. The selected area electron diffraction (SAED) pattern in Figure 1(i) provides additional confirmation of polycrystalline Ge in the sample. The electron diffraction pattern reveals continuous concentric circular diffraction rings corresponding to the (111), (220) and (331) crystal planes, consistent with the XRD results. Figure 1(j) displays the STEM and associated elemental mapping images of Ge@C(H_2/Ar) nanocomposites, showcasing the distribution of Ge and C elements. These images confirm the uniform dispersion of Ge nanoparticles and carbon-wrapped core-shell structure.[12] This is because both F127 and acetylene black prevented the agglomeration of Ge grains during pyrolysis.

Besides Ge@C(H_2/Ar), the GeO_2/F127 and acetylene black mixture was also pyrolized under nitrogen atmosphere to obtain Ge@C(N_2) for comparison. Figure 2(a) provides the XRD patterns of Ge, Ge@C(N_2) and Ge@C(H_2/Ar). These diffraction peaks fit well with the standard card of Ge (PDF#04-0545), indicating that GeO_2 has been completely transformed into Ge in the reduction process.[13] The characteristic diffraction peaks of carbon was not found, which is mainly masked by strong Ge diffraction peaks. The Raman spectra of Ge@C(H_2/Ar) and

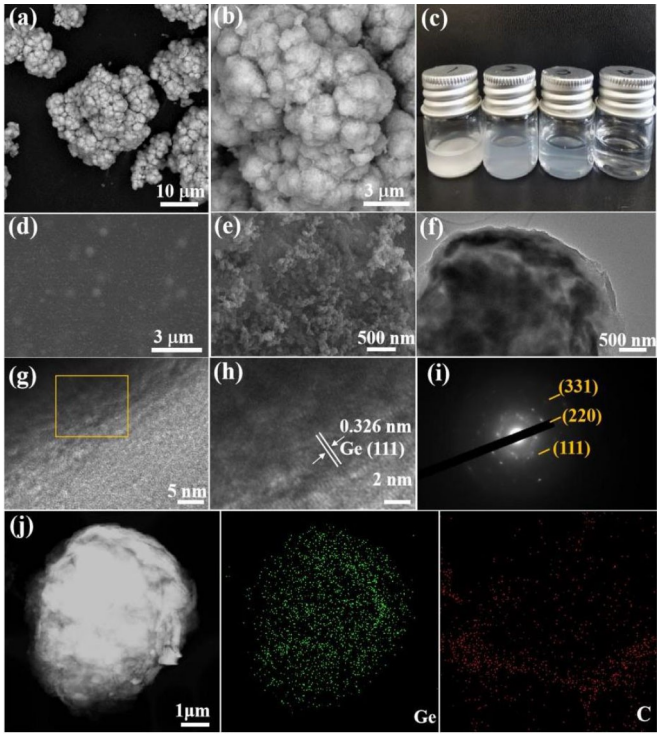

Figure 1. (a, b) SEM images of commercial GeO_2 polycrystalline microparticles; (c) Digital photograph of F127/GeO_2 dispersion: From left to right are dispersion with F127 concentration 0 wt%, 1 wt%, 2 wt% and 4 wt%; (d) SEM image of F127/GeO_2 nanocomposites obtained at 4 wt% F127 concentration; (e) SEM image of Ge@C(H_2/Ar); (f) TEM image of Ge@C(H_2/Ar); (g, h) HRTEM mages of Ge@C(H_2/Ar); (i) SAED pattern of Ge@C(H_2/Ar); (j) STEM and associated elemental mapping images of Ge@C(H_2/Ar).

Research Article
doi.org/10.1002/batt.202400139
Chemistry Europe
European Chemical Societies Publishing

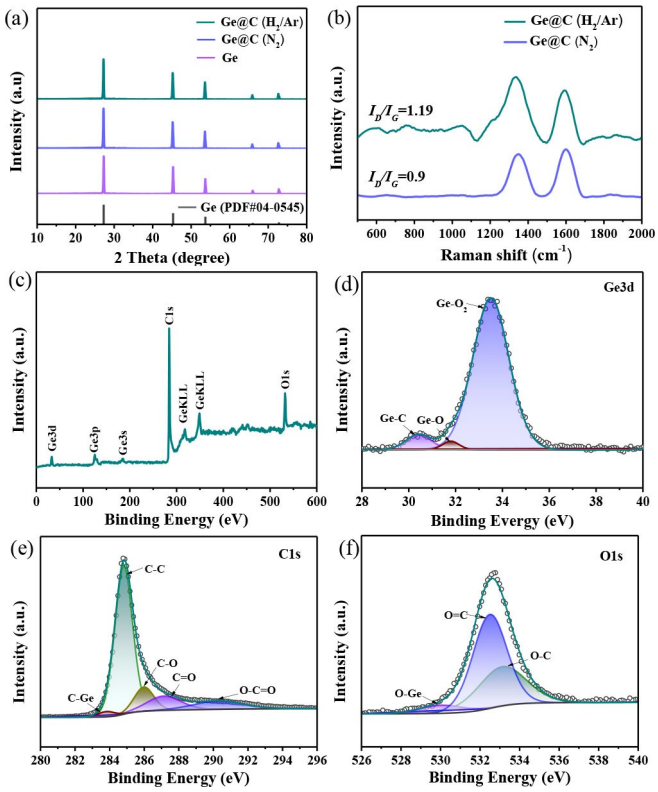

Figure 2. (a) XRD patterns of Ge@C(H_2/Ar), Ge@C(N_2) and Ge; (b) Raman spectra of Ge@C(H_2/Ar) and Ge@C(N_2); (c–f) XPS spectrum of Ge@C (H_2/Ar): (c) Survey spectrum, (d) Ge 3d, (e) C 1s, (f) O 1s.

Ge@C(N_2) in Figure 2(b) affirm the presence of carbon and provide insights into its level of disorder. Two carbon bands appear at 1320 cm^{-1} and 1600 cm^{-1}, corresponding to the D band (indicative of disordered carbon) and G band (representing ordered graphitic carbon).[14] Ge@C(H_2/Ar) exhibits a higher I_D/I_G value of 1.19 compared to that of Ge@C(N_2) (0.9), which indicates that hydrogen reduction can produce a higher proportion of disordered carbon and abundant defects,[15] which facilitates the diffusion kinetics of Li^+.[16] To further investigate the chemical composition of Ge@C(H_2/Ar) nanocomposites, XPS was employed to characterize the elements and their valence states in the material. The prominent peaks in the full spectrum shown in Figure 2(c) correspond to the characteristic peaks of C 1s, O 1s, Ge (3d, 3p, 3s) and Ge KLL. The Ge 3d peak is fitted into three peaks (Ge–C, Ge–O, Ge–O_2), corresponding to signals at 30.3, 31.8 and 33.5 eV, respectively, as illustrated in Figure 2(d). The Ge–C bond signifies that carbon atoms are randomly bonded to the Ge through sp3 hybridization, forming a stable carbon layer. The stable carbon layer serves as a basic protective structure, buffering the volume changes of Ge and acting as excellent electrical conductor to enhance electrical conductivity.[17] The presence of Ge–O bonds may be attributed to the oxidation of Ge nanoparticles on the surfaces of Ge@C(H_2/Ar) nanocomposites.[18] Figure 2(e) presents the high-resolution spectrum of C ls, revealing a strong peak at 284.8 eV (C–C) and three weak peaks at 284, 286, 287 and 290 eV, corresponding to C–Ge, C–O, C=O and O–C=O, respectively.[19] In Figure 2(f), the high-resolution spectrum of O1s illustrates the impact of oxygen, possibly arising from the oxidation of Ge@C(H_2/Ar) nanocomposites in air.

The Ge, Ge@C(N_2) and Ge@C(H_2/Ar) were assembled into CR2032 half-cell LIBs as anode materials. The Ge@C(H_2/Ar) anode was tested by CV at a scan rate of 0.2 $mV s^{-1}$. As presented in Figure 3(a), the CV curve shows an irreversible cathodic peak at 0~0.5 V during the first discharge, which is ascribed to the formation of solid electrolyte interface layer on the surface. In the following charging process, an anodic peak at 0.59 V is observed, which corresponds to the dealloying of Li_xGe. In the second cycle, the principal anodic peak persists at 0.59 V, while cathodic peaks emerge at 0.34 V and 0.21 V. These cathodic peaks are associated with the formation of Li–Ge phase alloy during the lithium alloying reaction.[20] These peaks remain stable across subsequent cycles, suggesting the highly reversible lithiation/delithiation of Ge@C(H_2/Ar) as an anode material for LIBs. Figure 3(b) displays the charge-discharge curves of Ge@C(H_2/Ar) at a constant current density of 0.1 $A g^{-1}$. The platforms observed during charge and discharge align with the positions of redox peaks illustrated in Figure 3(a). The initial discharge and charge capacities of the Ge@C(H_2/Ar) anode are 1700 $mA h g^{-1}$ and 1100 $mA h g^{-1}$, respectively. Subsequent discharge curves for the second and third cycles maintain a consistent capacity of about 1100 $mA h g^{-1}$, demonstrating excellent reversibility.

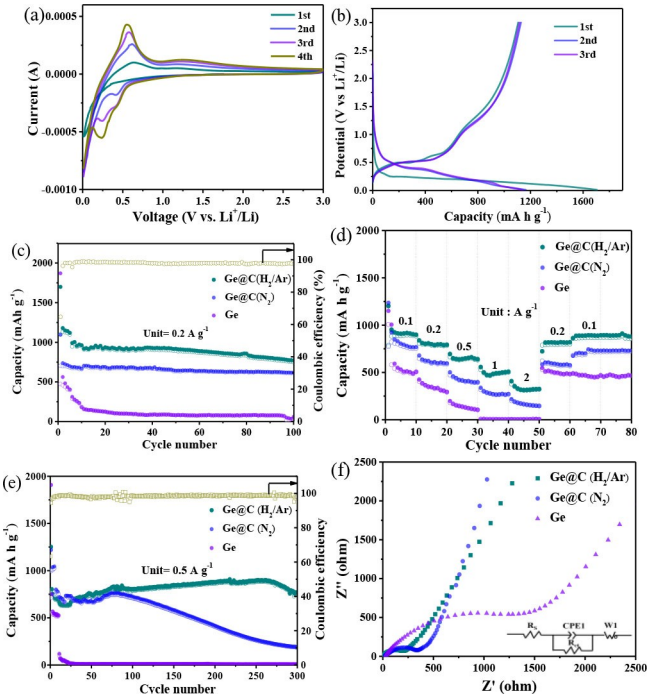

Figure 3. (a) CV curves of Ge@C(H_2/Ar) anode; (b) Charge-discharge curves of Ge@C(H_2/Ar) anode at 0.1 $A g^{-1}$; (c) Cycling performances of Ge, Ge@C(N_2) and Ge@C(H_2/Ar) anodes at 0.2 $A g^{-1}$; (d) Rate performances of Ge, Ge@C(N_2) and Ge@C(H_2/Ar) anodes at various current densities; (e) Cycling performances of Ge, Ge@C(N_2) and Ge@C(H_2/Ar) anodes at 0.5 $A g^{-1}$; (f) Nyquist plots of Ge, Ge@C(N_2) and Ge@C(H_2/Ar) anodes before cycling (inset: equivalent circuit).

Research Article
doi.org/10.1002/batt.202400139
Chemistry Europe
European Chemical Societies Publishing

Long-term cycle tests conducted at 0.2 A g^{-1} reveal that the Ge@C(H_2/Ar) anode maintains a stable capacity of 780 mAh g^{-1} after 100 cycles, outperforming Ge@C(N_2) and Ge anodes, as shown in Figure 3(c). In brief, Ge@C(H_2/Ar) anode exhibits superior cycling performance with a high discharge capacity and capacity retention rate across 100 cycles, which could be ranked as excellent Ge-based LIB anodes compared to literature results (Table S1). In contrast, the Ge anode experiences rapid capacity decay after several cycles, which is primarily attributed to the large volume expansion of Ge without protective carbon layer during cycling (Figure S2). The differences in cycling performance and coulombic efficiency between Ge@C(H_2/Ar) and Ge@C(N_2) anodes are related to the reduction degree of GeO_2 and the defects in Ge@C. Figure 3(d) displays the rate performance of Ge, Ge@C(N_2) and Ge@C(H_2/Ar) anodes at various current densities. As the current gradually increases from 0.1 to 0.2, 0.5, 1 and 2 A g^{-1}, the stable discharge capacities of Ge@C(H_2/Ar) are 916, 802, 633, 493 and 313 mAh g^{-1}, respectively. When the current density returns to 0.1 A g^{-1}, the discharge capacity of Ge@C(H_2/Ar) anode returns to 900 mAh g^{-1}. These results demonstrate that Ge@C(H_2/Ar) as anode materials has excellent rate performance, superior to that of Ge@C(N_2) and Ge. Figure 3(e) displays long-term cycle performance at 0.5 A g^{-1}. Obviously, the Ge@C(H_2/Ar) anode has superior long-term cycle performance with discharge capacities of 802 mAh g^{-1} and 767 mAh g^{-1} after the 2nd and 300th cycles, maintaining a high capacity retention rate of 95.6% and a consistently high coulombic efficiency. Figure 3(f) shows the Nyquist plots of Ge, Ge@C(N_2) and Ge@C(H_2/Ar) anodes before cycling with detailed fitting data shown in Table S2. All plots consist of a line in the low-frequency region and a half-circle in the high-frequency region, representing the ion-diffusion process and the charge-transfer resistance, respectively. The Ge@C-(H_2/Ar) anode shows a relatively small semicircle, indicating a small charge transfer resistance. This suggests a shortened electron transporting path and improved Li^+ diffusion efficiency,[21] contributing to the overall enhanced electrochemical performance of the Ge@C(H_2/Ar) anode.

The lithium storage kinetics of Ge@C(H_2/Ar) anode are further evaluated by CV at scan rates ranging from 0.2 to 1.0 mV s^{-1}. As displayed in Figure 4(a), all CV curves have similar shapes with minimal peak shifts, which indicate that the Ge@C(H_2/Ar) anode possesses exceptional lithiation/delithiation capabilities, supporting continuous charge and discharge processes. The relationship between scan rate (v) and peak current (i) is expressed by the formula: $i = av^b$, where the values of a and b may vary. The value of b, determined through a mathematical fit of log(i) and log(v), characterizes the electrochemical process. A b value between 0.5 and 1.0 suggests a combined mechanism of ion diffusion and Faraday capacitor behavior.[22] In Figure 4(b), the b values obtained by linear fitting of the cathodic and anodic peaks are approximately 0.68 and 0.93, which indicates that the conversion reaction process of Ge@C(H_2/Ar) anode is predominantly controlled by capacitive behavior. Additionally, capacitance contribution (k_1v) and diffusion contribution ($k_2v^{0.5}$) can be quantitatively determined using the formula: $i = k_1v + k_2v^{0.5}$. Figure 4(c) reveals that the

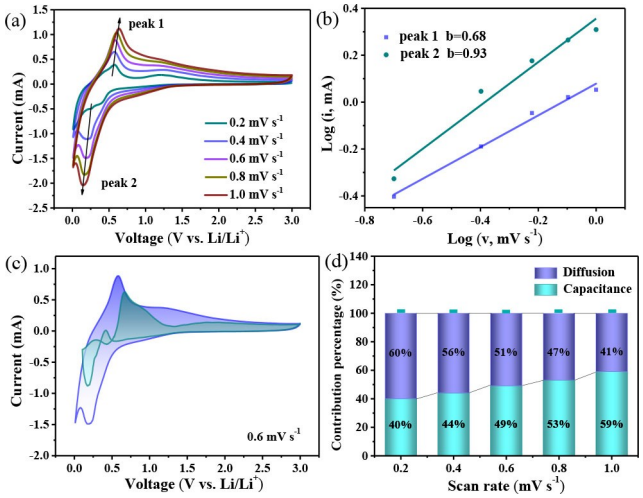

Figure 4. Kinetic analysis of Ge@C(H_2/Ar) anode: (a) CV curves at different scan rates; (b) Plots of log(i) against log(v); (c) Capacitive contribution to the total current at 1.0 mV·s^{-1}; (d) Capacitance contribution at different scan rates.

pseudocapacitance of Ge@C(H_2/Ar) anode accounts for approximately 49% of the total capacity at a scan rate of 0.6 mV s^{-1}. As illustrated in Figure 4(d), when the scan rates are 0.2, 0.4, 0.6, 0.8 and 1.0 mV s^{-1}, the capacitance control ratios are 40%, 44%, 49%, 53% and 59%, respectively. This suggests that the pseudocapacitance contribution becomes more significant with higher scan rates, indicating that the structure of Ge@C(H_2/Ar) anode is advantageous for achieving fast kinetics.[23]

Conclusions

In summary, we reveal that F127 could effectively disperse GeO_2 polycrystalline particles, which facilitates the preparation of Ge@C nanocomposites with the aid of acetylene black. The results demonstrated that GeO_2 polycrystalline microparticles were successfully broken down and completely reduced to Ge. The Ge nanoparticles were uniformly dispersed in acetylene black. When evaluated as anode material for LIBs, Ge@C(H_2/Ar) exhibited superior lithium storage performance than Ge@C(N_2). The Ge@C(H_2/Ar) anode exhibited excellent cycling stability and rate performance, boasting a high specific discharge capacity of 767 mAh g^{-1} after 300 cycles at 0.5 A g^{-1}, and a discharge capacity of 313 mAh g^{-1} at 2 A g^{-1}. The enhanced lithium storage performances were attributed to the combined effect of small-sized Ge nanoparticles, carbon coating and the presence of abundant defects. These factors collectively mitigated volume changes and improved the conductivity of the anode material, contributing to its exceptional cycling stability and rate capability.

Experimental Section

Chemicals and Reagents

Polyether F127 ($H(OCH_2CH_2)_x(OCH_2CHCH_3)_y(OCH_2CH_2)_zOH$) was procured from Shanghai Macklin Biochemical Co., Ltd. Germanium dioxide (GeO_2), acetylene black and carboxymethyl cellulose ($C_6H_{12}O_6 \cdot C_2H_4O_2$) were purchased from Sinopharm Group Co., Ltd. Deionized water was self-made in the laboratory.

Preparation of Ge@C Nanocomposites

Firstly, 0.4 g polyether F127 was dissolved in 20 mL deionized water to prepare F127 solution with a mass concentration of 2 wt%. 0.1 g commercial polycrystalline GeO_2 with particles in micrometer size were added to the above F127 solution under constant stirring to obtain GeO_2/F127 dispersion. Next, 0.02 g acetylene black was put into the GeO_2/F127 dispersion under ultrasonic conditions. Then, the dispersion was continuously stirred for 2 h to obtain uniform black slurry, which was subsequently transferred to a freeze dryer and dried at −60 °C for 12 h to obtain the black precursor powder. At last, the black precursor was calcined in a tube furnace under nitrogen or hydrogen-argon ($v(H_2):v(Ar)=5:95$) mixed atmosphere. The temperature was increased to 800 °C at a heating rate of 5 °C min^{-1} and maintained constant for 3 h before cooling to room temperature. The as-obtained Ge@C nanocomposites were denoted as Ge@C(N_2) and Ge@C(H_2/Ar) nanocomposites, respectively. For comparison, pure Ge without C was also prepared by directly reducing commercial GeO_2 under H_2/Ar atmosphere using the same pyrolysis procedure as Ge@C(H_2/Ar).

Materials Characterizations

Field emission scanning electron microscopy (FESEM, JEOL JSM-7500F) and transmission electron microscopy (TEM, JEOL-2100F) were employed to observe the morphology and microstructure of the prepared samples. The composition and crystal structure were investigated by X-ray diffractometer (XRD, TD-6000, Xu-Kα X-ray). The graphitization degree was characterized by Raman spectroscopy (EdinburghRM5, λ = 514 nm). The valence states of surface elements were characterized by X-ray photoelectron spectroscopy (XPS, Thermo Fisher Scientific Escalab-250 Xi). The carbon content in Ge/C was estimated using thermogravimetric analysis (TGA, STA449F3 Jupiter).

Electrochemical Measurements

In this work, the active material (Ge@C(H_2/Ar) or Ge@C(N_2) or Ge), acetylene black and carboxymethylcellulose (CMC) were weighed and mixed according to the mass ratio of 8:1:1. Then, the mixed powder was grinded in an agate mortar for 30 min. After that, a certain amount of water was added to form black slurry after stirring overnight. The slurry was applied onto copper foil and subjected to vacuum-drying at 85 °C to eliminate moisture. The modified copper foil was then cut into discs with a 12 mm diameter, serving as anodes for LIBs. The loading capacity of the active material on a single electrode ranged from 1 to 1.2 mg. Finally, the prepared anode, lithium metal foil (Φ = 15.5 mm) and Celgard 2400 separator were assembled into coin-type half-cells (CR2032), in which 1 mol L^{-1} $LiPF_6$ dissolved in the mixed solvent of dimethyl carbonate and ethylene carbonate (1:1 volume ratio) was used as electrolyte. The entire assembly process took place within a glove box filled with inert gas. Cyclic voltammograms (CV) were recorded at a voltage window of 0.01~3 V on a CHI 760 electrochemical workstation. Electrochemical impedance spectroscopy (EIS) measurements were performed within the frequency range of 1×10^{-2}~1×10^{5} Hz. The charging-discharging behaviors of the batteries were investigated by the LAND battery test system (LAND CT-2001A).

Acknowledgements

This work was financially supported by National Natural Science Foundation of China (22379056, 52102100, 22022505), China Postdoctoral Science Foundation (2022M721545), Carbon Peak and Carbon Neutrality Project (Breakthrough for Industry Prospect and Key Technologies) of Zhenjiang City (CG2023003), Fundamental Research Funds for the Central Universities of China (020514380266, 020514380272 and 020514380274), Scientific and Technological Innovation Special Fund for Carbon Peak and Carbon Neutrality of Jiangsu Province (BK20220008), Scientific and Technological Achievements Transformation Special Fund of Jiangsu Province (BA2023037), International Collaboration Research Program of Nanjing City (202201007 and 2022SX00000955), and Gusu Leading Talent Program of Scientific and Technological Innovation and Entrepreneurship of Wujiang District in Suzhou City (ZXL2021273).

Conflict of Interests

The authors declare no conflict of interest.

Data Availability Statement

The data that support the findings of this study are available from the corresponding author upon reasonable request.

Keywords: germanium · nanoparticles · triblock polymer/acetylene black dual-assisted strategy · anode materials · lithium-ion batteries

[1] a) C. Y. Wang, T. Liu, X. G. Yang, S. H. Ge, N. V. Stanley, E. S. Rountree, Y. J. Leng, B. D. McCarthy, *Nature* **2022**, *611*, 485–490; b) X. Guo, J. Zhang, L. Yuan, B. Xi, F. Gao, X. Zheng, R. Pan, L. Guo, X. An, T. Fan, S. Xiong, *Adv. Energy Mater.* **2023**, *13*, 202204376; c) X. Wan, X. Guo, M. Duan, J. Shi, S. Liu, J. Zhang, Y. Liu, X. Zheng, Q. Kong, *Electrochim. Acta* **2021**, *394*, 139135.
[2] a) Z. Y. Ren, Z. Chen, H. Y. Huang, X. B. Zhang, R. Zhang, M. Y. Liu, P. T. Zhang, S. J. Li, *Electrochim. Acta* **2023**, *469*, 143244; b) K. Xue, Ya. Xue, J. Wang, S. Zhang, X. Guo, X. Zheng, F. Cao, Q. Kong, J. Zhang, Z. Jin, *Chin. J. Chem. Eng.* **2023**, *57*, 214–223; c) J. Wang, J. Chen, S. Zhang, K. Xue, J. Zhang, F. Cao, Q. Kong, X. Guo, *J. Alloys Compd.* **2023**, *935*, 167850.
[3] a) H. S. Choe, S. J. Kim, M. C. Kim, D. M. Kim, G. H. Lee, S. B. Han, D. H. Kwak, K. W. Park, *RSC Adv.* **2016**, *6*, 72926–72932; b) D. H. Tang, H. Yu, J. W. Zhao, W. T. Liu, W. T. Zhang, S. J. Miao, Z. A. Qiao, J. X. Song, Z. Zhao, *J. Colloid Interface Sci.* **2020**, *561*, 494–500.
[4] a) J. Chen, X. Guo, M. Gao, J. Wang, S. Sun, K. Xue, S. Zhang, Y. Liu, J. Zhang, *Chem. Commun.* **2021**, *57*, 10580–10583; b) H. Yu, M. Gao, M. Zhou, H. Gu, X. Zheng, X. Guo, Y. Liu, F. Cao, Q. Kong, J. Zhang, *J. Mater. Res. Technol.* **2023**, *26*, 5055–5064.
[5] R. W. Mo, Z. Y. Lei, D. Rooney, K. N. Sun, *ACS Nano* **2019**, *13*, 7536–7544.
[6] D. T. Ngo, H. T. T. Le, C. Kim, J. Y. Lee, J. G. Fisher, I. D. Kim, C. J. Park, *Energy Environ. Sci.* **2015**, *8*, 3577–3588.

[7] L. Y. Wang, M. Wang, L. S. Jiao, H. Q. Wang, J. H. Yang, X. Z. Dong, T. Bi, S. S. Ji, L. Liu, S. L. Hu, C. M. Chen, Q. G. Guo, Z. J. Liu, *Coating* **2023**, *13*, 555.
[8] S. W. Kim, D. T. Ngo, J. Heo, C. N. Park, C. J. Park, *Electrochim. Acta* **2017**, *238*, 319–329.
[9] J. Ryu, D. Hong, S. Shin, W. Choi, A. Kim, S. Park, *J. Mater. Chem. A* **2017**, *5*, 15828–15837.
[10] J. H. Zhang, T. T. Yu, J. L. Chen, H. L. Liu, D. Q. Su, Z. H. Tang, J. F. Xie, L. Chen, A. H. Yuan, Q. H. Kong, *Ceram. Int.* **2018**, *44*, 1127–1133.
[11] M. Huang, K. Mi, J. H. Zhang, H. L. Liu, T. T. Yu, A. H. Yuan, Q. H. Kong, S. L. Xiong, *J. Mater. Chem. A* **2017**, *5*, 266–274.
[12] X. Guo, J. Shi, M. Li, J. Zhang, X. Zheng, Y. Liu, B. Xi, X. An, Z. Duan, Q. Fan, F. Gao, S. Xiong, *Angew. Chem. Int. Ed.* **2023**, *62*, e202314124.
[13] H. Gu, M. Gao, T. Zhang, J. Zhang, X. Zheng, X. Guo, Y. Liu, F. Cao, Q. Kong, S. Xiong, *Chin. Chem. Lett.* **2023**, *35*, 109273.
[14] a) X. Guo, S. Liu, X. Wan, J. Zhang, Y. Liu, X. Zheng, Q. Kong, Z. Jin, *Nano Lett.* **2022**, *22*, 4879–4887; b) J. Shi, X. Guo, S. Liu, J. Zhang, Y. Liu, X. Zheng, Q. Kong, *Composites Part B* **2022**, *231*, 109589.
[15] W. Ai, N. Kirkaldy, Y. Jiang, G. Offer, H. Z. Wang, B. L. Y. Wu, *J. Power Sources* **2022**, *527*, 231142.
[16] T. Zhang, M. Wu, H. Gu, H. Yu, M. Zhou, X. Guo, Y. Liu, X. Zheng, Q. Kong, J. Zhang, *J. Energy Storage* **2023**, *73*, 108981.
[17] M. Gao, Z. Tang, M. Wu, J. Chen, Y. Xue, X. Guo, Y. Liu, Q. Kong, J. Zhang, *J. Alloys Compd.* **2021**, *857*, 157554.
[18] X. Guo, M. Duan, J. Zhang, B. Xi, M. Li, R. Yin, X. Zheng, Y. Liu, F. Cao, X. An, S. Xiong, *Adv. Funct. Mater.* **2022**, *32*, 2209397.
[19] X. Guo, J. Xie, J. Wang, S. Sun, F. Zhang, F. Cao, Y. Liu, X. Zheng, J. Zhang, Q. Kong, *Chin. J. Chem. Eng.* **2022**, *52*, 88–94.
[20] A. N. Sosa, I. Gonzalez, A. Trejo, A. Miranda, F. Salazar, M. Cruz-Irisson, *J. Comput. Chem.* **2020**, *41*, 2653–2662.
[21] M. Wu, M. Gao, S. Zhang, R. Yang, Y. Chen, S. Sun, J. Xie, X. Guo, F. Cao, J. Zhang, *Int. J. Min. Met. Mater.* **2021**, *28*, 1656–1665.
[22] M. Gao, Y. Xue, Y. Zhang, C. Zhu, H. Yu, X. Guo, S. Sun, S. Xiong, Q. Kong, J. Zhang, *Inorg. Chem. Front.* **2022**, *9*, 3933–3942.
[23] Y. Xue, X. Guo, M. Wu, J. Chen, M. Duan, J. Shi, J. Zhang, F. Cao, Y. Liu, Q. Kong, *Nano Res.* **2021**, *14*, 3598–3607.

Manuscript received: March 1, 2024
Revised manuscript received: April 3, 2024
Accepted manuscript online: April 9, 2024
Version of record online: May 2, 2024